

Article

Experimental Study on Mechanical Properties of Rectangular Reinforced Concrete Pipe with Corrosion Defects

Zhe Mei , Peng Zhang  and Cong Zeng *

Faculty of Engineering, China University of Geosciences, Wuhan 430074, China; meizhe198@163.com (Z.M.);
cugpengzhang@163.com (P.Z.)

* Correspondence: zengcong@126.com

Abstract: Rectangular reinforced concrete pipes are widely used in various municipal projects. Because they are often located in weak strata in urban areas, they are prone to structural defects such as corrosion, which in turn leads to a decline in the bearing capacity of reinforced concrete pipes and, in severe cases, causes disasters such as pipe collapse. In this paper, the mechanical properties of rectangular reinforced concrete pipes with corrosion defects are studied through laboratory tests, and the influence of the pipe failure mechanism and corrosion depth on the ultimate bearing capacity of pipes is analyzed. A numerical simulation method is used to verify the test results, and the numerical simulation results are in good agreement with the indoor test results. The research shows that the failure mode of rectangular reinforced concrete pipe under TEB test conditions can be divided into an uncracked stage, a crack development stage and a failure stage. With the increase of corrosion depth, the ultimate bearing capacity of the pipe decreases. When the corrosion depth is equal to the thickness of the protective layer, the ultimate bearing capacity of the pipe is more than 30%, and the corrosion depth has a great influence on the mechanical properties of the pipe.

Keywords: reinforced concrete pipes; corrosion; mechanical properties; load test



Citation: Mei, Z.; Zhang, P.; Zeng, C. Experimental Study on Mechanical Properties of Rectangular Reinforced Concrete Pipe with Corrosion Defects. *Appl. Sci.* **2023**, *13*, 7570. <https://doi.org/10.3390/app13137570>

Academic Editor: Motoharu Fujigaki

Received: 15 May 2023

Revised: 11 June 2023

Accepted: 25 June 2023

Published: 27 June 2023



Copyright: © 2023 by the authors. Licensee MDPI, Basel, Switzerland. This article is an open access article distributed under the terms and conditions of the Creative Commons Attribution (CC BY) license (<https://creativecommons.org/licenses/by/4.0/>).

1. Introduction

Reinforced concrete pipe is a kind of reinforced concrete structure, which is a fully enclosed underground structure with the functions of accommodation, transportation and watercrowning. It is also one of the common forms of urban underground space utilization [1]. Reinforced concrete pipes have the advantages of high construction accuracy, high structural strength, good safety and durability. They are widely used in underground crossings, utility pipes, power pipes, and water supply and drainage pipes. They are an important part of municipal infrastructure [2].

Reinforced concrete pipes are often located in weak strata in urban areas with complex geological conditions. Their own structures often have defects such as corrosion defects and cracks. As time goes by, their materials have the risk of deterioration and have certain safety hazards [3]. Studying the mechanical properties of in-service reinforced concrete pipe structures can provide a scientific basis for quantitative evaluation of structural health status, and provide a theoretical basis for subsequent maintenance and repair [4].

Compared with circular reinforced concrete pipes, rectangular reinforced concrete pipes have the advantages of high space utilization, good stability and good foundation applicability [5]. However, for rectangular reinforced concrete pipes, the difference in cross-section shape leads to differences in the force form, failure mode and bearing capacity analysis method of the two in the stratum [6]. At present, research on the mechanical behaviors of rectangular reinforced concrete pipes with corrosion defects, at home and abroad, mostly considers the influence of the concentration and diffusion law of microscopic particles such as chloride ions on the compressive strength of concrete and the tensile and compressive strength of steel bars. Although the relevant research accurately explains the

corrosion mechanism of corrosive media on reinforced concrete materials, it lacks focus on the overall mechanical properties of reinforced concrete structures under corrosion conditions [7,8].

In summary, there are few studies on the overall mechanical properties of rectangular reinforced concrete pipe structures with corrosion defects [9]. In this paper, an external pressure load test is carried out on rectangular reinforced concrete pipe with corrosion defects, and the influence law of bearing capacity of pipe with different corrosion depths is determined by numerical simulation.

2. TEB Test of Corroded Pipe

2.1. Test Ideas

In this section, an external pressure load test was carried out on rectangular reinforced concrete pipe to study the influence of different defects on the bearing capacity of pipe. In order to achieve this, a three-edge bearing (TEB) test was carried out on pipes with different corrosion depths [10]. The load-displacement curve of the pipe was obtained by arranging the displacement meters in the vertical and horizontal directions of the pipe. The test results were analyzed, and the failure law of the corrosion defect pipe was obtained. The mechanical performance test of rectangular reinforced concrete pipe with corrosion defects mainly studies the influence of corrosion depth on the bearing capacity of pipe. Four groups of tests were set up according to the thickness of the inner protective layer of the pipe, and the key parameters of the defective pipe structure with the corrosion depth of 1/3, 2/3 and 1 of the thickness of the inner protective layer of the pipe were measured.

2.2. Test Method and Process

2.2.1. Pipe Pouring and Pretreatment

The pipes used in the test were all artificially poured. The cross-sectional dimensions of the rectangular pipe were $a \times b = 500 \text{ mm} \times 400 \text{ mm}$, the length of the pipe was 100 mm, and the thickness of the pipe was 60 mm. All pipe samples were made from molds. The cement ash and aggregate were stirred evenly and then slowly added to water. The water-cement ratio was 0.38 and the sand-cement ratio was 1.2. The mixed concrete was poured into the mold with a steel cage placed in advance, quickly and evenly, and the bubble inside the concrete was removed by a vibrating machine. After pouring and demolding, the curing conditions were natural curing for 28 days.

After the pipe maintenance was completed, the pipe was pretreated. Group A1 pipe did not need to be treated, and B1, B2 and B3 needed to have the inner wall of the pipe thinned. As shown in Table 1 and Figure 1, different sizes of internal molds were used to realize the thinning of the inner wall of the pipe. The internal mold of the pipe adopts customized fixed-size high-density cubic foam. There are three reasons for not using artificial chiseling and chemicals to corrode the inner wall protective layer of concrete pipes: (1) The chemical corrosion process has a high risk, a long corrosion cycle and huge cost; (2) It is difficult to accurately control the corrosion depth and achieve the same corrosion depth at each point with chiseling and chemical corrosion; (3) The chemical corrosion process will affect the mechanical properties of steel bars and concrete. Other defects can easily occur in the process of artificial chiseling, which may also cause damage to the pipe structure and cannot meet the single variable assumption of corrosion depth explained in the previous section.

Table 1. Corrosion defect pipe test table.

| Test Serial Number | Defect Type | Defection Evaluation | Number |
|--------------------|-------------|--|--------|
| A1 | Undamaged | Nil | 1 |
| B1 | Corrosion | The corrosion depth is 1/3 protective layer thickness. | 1 |
| B2 | Corrosion | The corrosion depth is 2/3 protective layer thickness. | 1 |
| B3 | Corrosion | The corrosion depth is 1 protective layer thickness. | 1 |

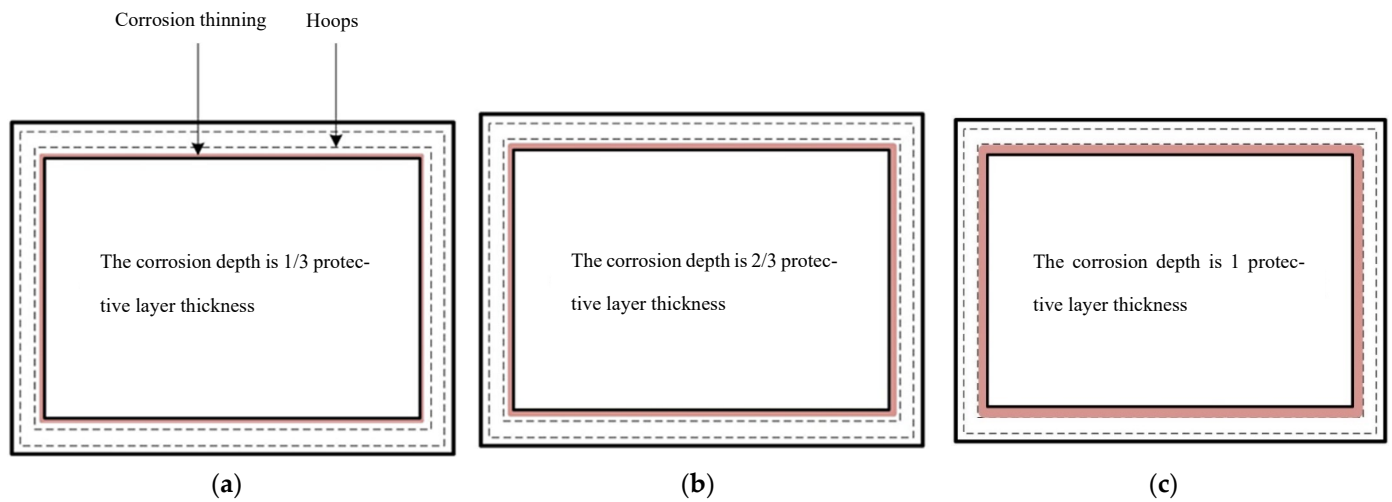


Figure 1. Schematic diagram of corrosion defective pipe: (a) The corrosion depth is 1/3 protective layer thickness; (b) The corrosion depth is 2/3 protective layer thickness; (c) The corrosion depth is 1 protective layer thickness.

2.2.2. Acquisition of Pipe Physical and Mechanical Parameters

After the pipe is preprocessed, the physical and mechanical parameters of the pipe need to be measured by non-destructive testing to provide specific parameters for the subsequent numerical simulation of the mechanical properties of the pipe. The parameters and testing instruments used for these measurements are shown in Table 2.

Table 2. Pipe measurement parameters and testing instruments.

| Test Parameter | Detecting Instrument |
|----------------------------------|---|
| Pipe appearance size | Band tape |
| Pipe concrete strength | HT-225T resiliometer, HC-U81 concrete ultrasonic detector |
| Thickness of reinforcement cover | HC-GY71T integrated steel bar scanner |
| Steel reinforcement diameter | Vernier caliper, HC-GY71T integrated steel bar scanner |
| Crack opening | Vernier caliper, crack width gauge |
| Crack length | Band tape |
| Crack depth | Ultrasonic detector |

2.2.3. Displacement Measurement

Two LVDT displacement sensors were used to measure the horizontal and vertical displacement changes of the pipe. The displacement sensors were installed using a universal magnetic clamp with a range of 30 mm. The sensor placement method is shown in Figure 2, and the displacement sensor data were collected in real time through a static strain acquisition system.

2.2.4. Loading and Data Acquisition

Before loading, a PIV photogrammetry device should be applied to measure the crack propagation and section change of pipe. The ring stiffness machine is used to realize the graded loading of the pipe by controlling the displacement. The pipe force model is shown in Figure 3. The loading speed was 3 mm/min at 0–5 kN, and then decreased to 1 mm/min. Loading was stopped after the pipe was damaged, and steps 2–4 were repeated after removing the pipe.

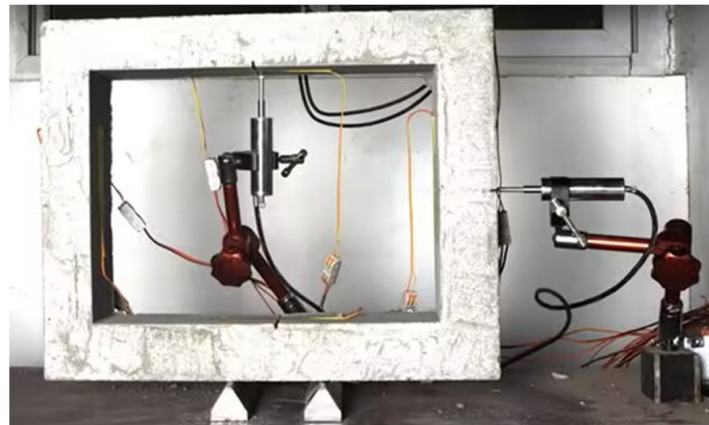


Figure 2. Pipe displacement sensor layout.

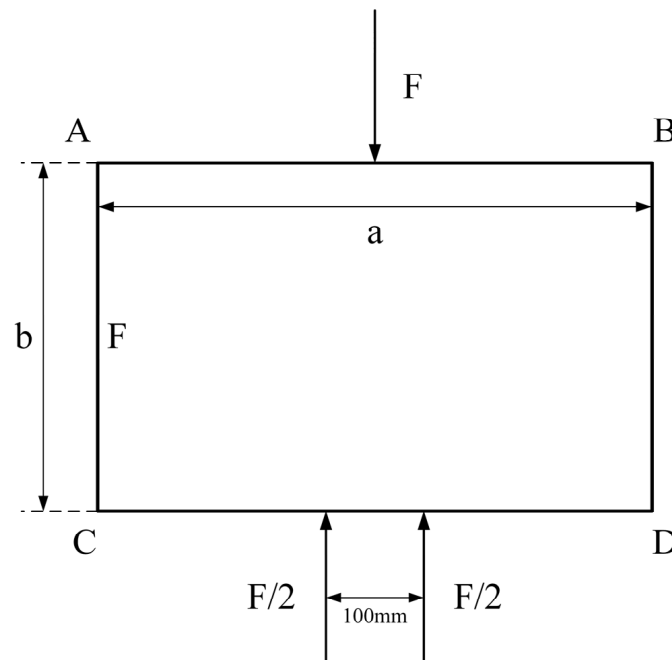


Figure 3. Pipe force model.

2.3. Test Results and Analysis

2.3.1. Sample Failure Mode

In this section, the failure modes of pipes under different working conditions are compared. The load-displacement curves and crack development of group A1 non-destructive rectangular reinforced concrete pipes are shown in Figures 4 and 5. Comparing the load-displacement curves of four groups of pipes with different corrosion depths, the curve changes are roughly the same, and the pipe deformation is divided into three stages, The uncracked stage, the crack development stage and the failure stage [11]. The stress characteristics of pipe concrete and internal steel bars in each stage were analyzed, and the reasons for the change rule of the key point curve were summarized.

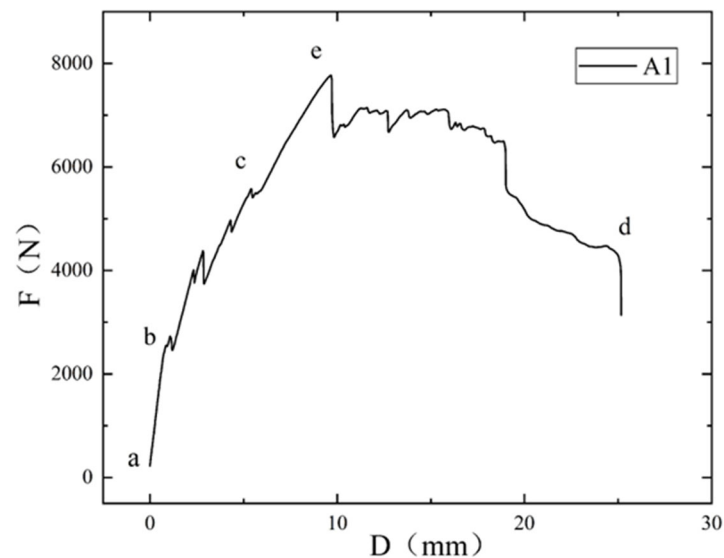


Figure 4. A1 pipe load-displacement curve.

1. Uncracked stage.

Point a is the starting point. At this time, the upper steel bar of the ring stiffness machine contacts the A1 group pipe crown. The displacement of the ring stiffness machine can be regarded as the downward displacement of the pipe crown mid-span. The pipe is subjected to the pressure exerted by the ring stiffness machine, as shown in Figure 5a. Between point a and point b is the uncracked stage, before concrete cracking. The load on the pipe at this stage increases with the increase of the displacement of the ring stiffness machine, and the overall law is linear. The working condition of the component is similar to that of the homogeneous elastic beam. The compressive area of concrete is in the elastic working stage, and the strain of concrete at the edge of the tensile area increases rapidly, showing plastic characteristics. Due to the large cohesive force between concrete and steel bars, the strain of steel bars in concrete is the same as that of concrete at the same level. The pipe uncracked stage has the following characteristics: (1) At this stage, the concrete is not cracked and the deflection is small; (2) The stress curve of concrete in the tension zone is straight in the early stage and curved in the later stage.

2. Crack development stage.

Point b is the initial time of concrete cracking, as shown in Figure 5b. Cracks first appear in the dangerous section (the middle of the pipe crown and the stress concentration area of the bottom). The crack develops from the tensile area to the compressive area, and gradually forms a penetrating crack, but the crack width is small. The bearing capacity corresponding to point b can be used as the theoretical basis for the calculation of pipe crack resistance. Between point b and point c is the crack development stage, after concrete cracking. At this stage, concrete cracks increase, and concrete is a brittle material. After cracks occur, they should develop rapidly and cause damage. However, some of the tension originally borne by concrete is transferred to the steel bars inside the concrete, and the stress and strain of the steel bars increases. In Figure 4, the load on the pipe in the crack development stage increases with the increase of displacement, but the slope of the curve is smaller than that in the first stage. The reason may be that the concrete in the compression zone has plastic deformation at this stage, and the concrete strain increases faster. The crack development stage has the following characteristics: (1) The concrete in the tensile zone at the crack of the pipe is deactivated, and the concrete only exhibits compressive performance; (2) The tension at the crack is borne by the steel bar, but the steel bar does not reach the yield state; (3) Plastic deformation occurs in the concrete of the compression zone,

but this is not sufficient. Point c is the normal stress state of the pipe, which is often used as the theoretical basis for deformation checking in normal use stage.

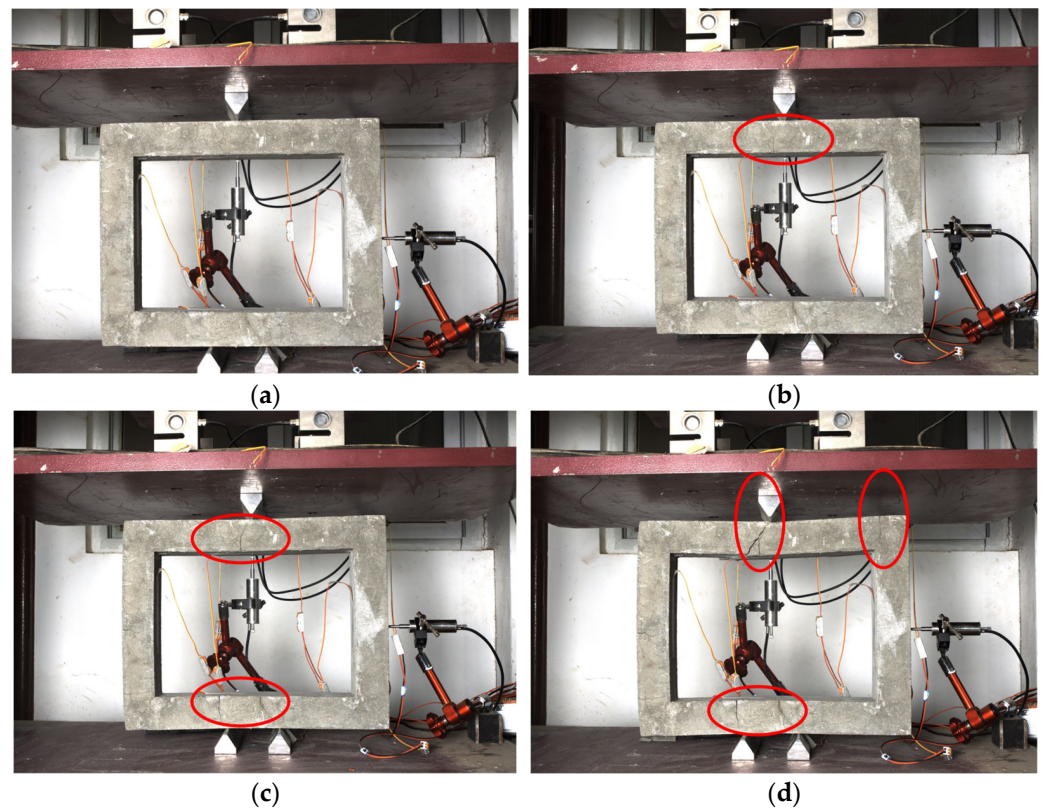


Figure 5. A1 pipe crack development situation: (a) Start loading on pipe; (b) Cracks appear on pipe crown; (c) Cracks appear on pipe crown and bottom; (d) Pipe is damaged.

3. Failure stage.

From point c to point d is the pipe failure stage. At this stage, the steel bar yields, the pipe deforms greatly, the deflection of the pipe crown and the curvature of the mid-span section increase, the crack width increases, and the area of the outer compression area of the pipe crown becomes smaller. The reason for the load strengthening from point c to point e may be that a certain amount of elastic strain energy is accumulated during the pre-compression process of concrete. This elastic strain energy is greater than the energy required for crack development, resulting in rapid development of cracks. At the same time, the steel bars in the concrete do not reach the yield limit, the tensile stress of the steel bars continues to increase, and the internal stress of the pipe increases [12]. The load of the pipe at point e reaches the maximum value, and the corresponding load is the ultimate bearing capacity of the pipe. The displacement of point e is 9.65 mm, and the ultimate bearing capacity of the pipe is 8091.35 N. Then, the load value of the pipe changes abruptly, and pipe brittle failure occurs, as shown in Figure 5c. Cracks appear in the mid-span of the pipe crown and the stress concentration area of the bottom plate. The pipe structure is damaged and the pipe loses its bearing capacity. After reaching the highest point e, it enters the descending stage. At this time, the cracks continue to develop, expand and penetrate, and the concrete is crushed. At point e, the load suddenly drops, and then a nearly horizontal curve appears. The reason for this curve is that the steel bar reaches the yield strength at this time, and the tensile force remains constant. The concrete is continuously crushed, and the bearing capacity of the pipe is mainly borne by the steel bar. At this time, the deformation degree of the pipe is intensified and the load is almost unchanged. At point d, the crack is widened, the steel bar strain continues to increase, the steel bar is broken, and the pipe structure is completely destroyed, as shown in Figure 5d. The B1 corrosion defect

pipe is roughly the same as the A1 non-destructive pipe, and the ultimate bearing capacity and crack development law will be discussed later.

2.3.2. Influence of Corrosion Depth on Ultimate Bearing Capacity of Pipe

The corrosion defect rectangular reinforced concrete pipe mainly considers the influence of corrosion depth on the ultimate bearing capacity of the pipe. Figure 6 is the load-displacement curve of non-destructive and corrosion defect pipe, where e_0 , e_1 , e_2 and e_3 represent the ultimate bearing capacity of A1 non-destructive pipe, B1 corrosion defect pipe, B2 corrosion defect pipe and B3 corrosion defect pipe, respectively. The specific data are shown in Table 3. According to the data in the table, the ultimate bearing capacity of the pipe decreases with the increase of the corrosion depth, and the displacement corresponding to the ultimate bearing capacity increases with the increase of the corrosion depth. When the corrosion depth reaches the thickness of the protective layer, the ultimate bearing capacity of the pipe is reduced by 38%, which proves that the corrosion depth has a great influence on the ultimate bearing capacity of the pipe.

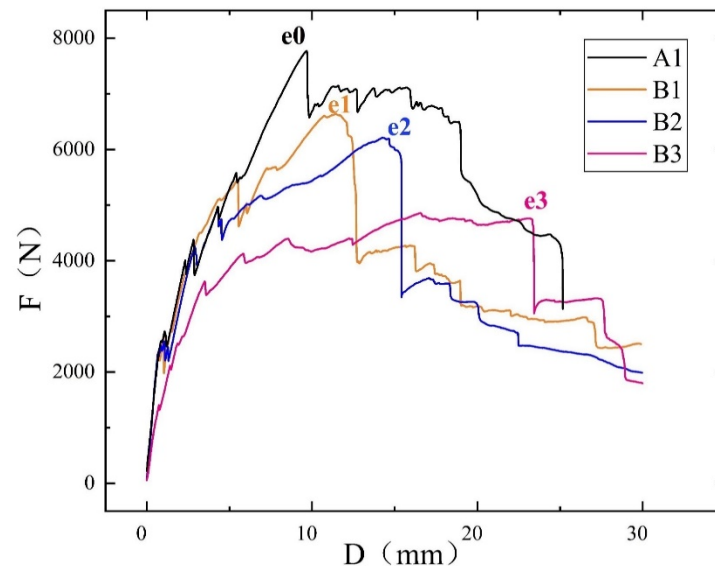


Figure 6. Load-displacement curves of pipe with non-destructive and corrosion defects.

Table 3. Ultimate bearing capacity of corroded pipe.

| Serial Number | The Ultimate Bearing Capacity Corresponds to the Displacement (mm) | Ultimate Bearing Capacity (N) |
|---------------|--|-------------------------------|
| A1 | 9.65 | 7768.24 |
| B1 | 10.73 | 6610.76 |
| B2 | 14.25 | 6212.21 |
| B3 | 16.79 | 4801.54 |

3. Numerical Simulation Study on Mechanical Properties of Corroded Pipe

3.1. Numerical Simulation Steps

In this section, ABAQUS finite element analysis software is used to simulate the bearing capacity of non-destructive and corroded rectangular reinforced concrete pipes under TEB test conditions. The specific steps are as follows:

1. Modeling.

According to the geometric parameters of the A1, B1, B2 and B3 groups of pipes, the concrete and steel cage models are established. According to the design requirements, the geometric parameters of the non-destructive pipe are as shown in Table 4 (the wall thickness of the corrosion defect pipe is reduced according to the corrosion depth). The size

and position of the steel bar are consistent with the pouring pipe of the test group. Among them, the concrete parts are stretched by three-dimensional entities, and the steel cage is a line unit [13].

Table 4. A1 non-destructive pipe physical and mechanical parameters.

| Pipe Parameters | Numerical Value | Pipe Parameters | Numerical Value |
|-------------------------------------|-----------------|--------------------------------|-----------------|
| Average length | 440 mm | Stirrup tensile strength | 650 MPa |
| Average width | 340 mm | Stirrup compressive strength | 613 MPa |
| Tube length | 100 mm | Number of hoops | 1 |
| Wall thickness | 60 mm | Stirrup diameter | 5 mm |
| Inner protective layer thickness | 7.5 mm | Tensile reinforcement area | 19.625 mm |
| Thickness of outer protective layer | 7.5 mm | Compression reinforcement area | 19.625 mm |
| Concrete compressive strength | 23.4 MPa | | |

2 Give material properties.

The concrete component adopts the plastic damage model (CDP), and the steel cage component adopts the elastic–plastic model. The tensile strength, compressive strength and yield stress of each group of steel bar materials are shown in Table 4. The material properties used in the numerical simulation are shown in Table 5.

Table 5. Material properties.

| Material Properties | Numerical Value |
|---|------------------------|
| Modulus of elasticity for concrete | 31,500 MPa |
| Poisson ratio | 0.2 |
| Density | 2500 kg/m ³ |
| Expansion angle | 36° |
| Eccentricity | 0.1 |
| Ratio of initial equal biaxial compression yield stress to initial uniaxial compression yield stress | 1.16 |
| The maximum principal stress is any given value of the negative pressure invariant. Under the initial yield condition, the ratio of the second stress invariant on the tensile meridian to the second stress invariant on the compressive meridian. | 0.67 |
| Coefficient of viscosity | 0.0001 |

3 Component assembly.

The reinforced cage components with attributes are assembled into concrete components. The geometric space position of the steel bar should strictly correspond to the test group. The assembly method of the reinforced cage component and the concrete component is the built-in area constraint method [14].

4 Establish the analysis step, set the field output and the history output.

After assembly, the static analysis step is established and the convergence of the model is enhanced. Usually, the method of modifying the maximum number of continuous contractions (IA) in the incremental step in the solver is used to set up the reference point and establish the process output to derive the reaction force and displacement in the vertical direction.

5 Define constraints and apply loads.

In the TEB test, the pipe is subjected to linear load, and the ring stiffness loading device and the contact area of the pipe bottom plate are hinged. The contact area between the pipe crown and the ring stiffness loading device applies the numerical downward uniform linear displacement by displacement coupling.

6 Mesh subdivision.

The concrete components and steel cage components are divided into grids. The concrete components adopt C3D8 R element, which adopts reduced integration and hourglass control. The steel cage components adopt T3D2 row frame element. The linear reduced integration element has the following advantages: (1) When bending load is applied, the components generally do not appear self-locking phenomenon; (2) When the mesh is not standard or the mesh is distorted, the accuracy of the numerical simulation results is not greatly affected; (3) The displacement solution results are accurate. Before meshing, the datum plane is used to cut the geometric irregular area of the concrete component, so that the mesh is more accurate and the calculation accuracy is higher.

7 Computational solution.

The numerical simulation models are established and submitted, the calculation solved and the results exported.

The group A1 pipe is a non-destructive pipe, and the B1, B2, and B3 pipes all use the method of adjusting the model cross-section set parameters to achieve the reduction of the thickness of the inner protective layer of the pipe. In the four groups of simulations, except for the thickness of the inner protective layer of the pipe (corrosion depth), other physical and mechanical parameters are unchanged, ensuring the same assumptions as in the theoretical model, so as to compare the test results under the same conditions.

3.2. Numerical Simulation Results Analysis

3.2.1. Analysis of Numerical Simulation Results of Pipe Failure Mode

The maximum principal stress diagram and plastic strain cloud diagram of four groups of pipe mechanics are shown in Figures 7 and 8, respectively. The maximum principal stress of the A1 group, B1 group, B2 group and B3 group are shown in Figure 7a–d. It can be seen that, because the load on the pipe is symmetrical, the maximum stress of the pipe is symmetrically distributed. The tension zone and compression zone of the four groups of pipes are roughly the same, among which the upper crown and the inner side of the lower bottom plate are the tension zone, and the maximum tensile stress appears in the middle of the pipe crown and the bottom plate, which is consistent with the damage of the pipe in the upper section. The bottom and the middle of the top span are the dangerous sections under the TEB test conditions. At the same time, the outside of the pipe side is the tension area, and the compression area appears on the top of the pipe, the outside of the pipe bottom and the inner wall of the pipe side. Comparing the maximum principal stress diagrams of pipes with different corrosion depths, it is found that, with the increase of corrosion depth, the maximum tensile stress inside the pipe increases and the maximum compressive stress decreases, while the tensile resistance of concrete materials is extremely weak. It can be inferred that the corrosion depth of the pipe has an effect on the ultimate bearing capacity of the pipe. As the corrosion depth of the pipe increases, the ultimate bearing capacity of the pipe decreases and the pipe is more dangerous. This conclusion is consistent with the experimental results.

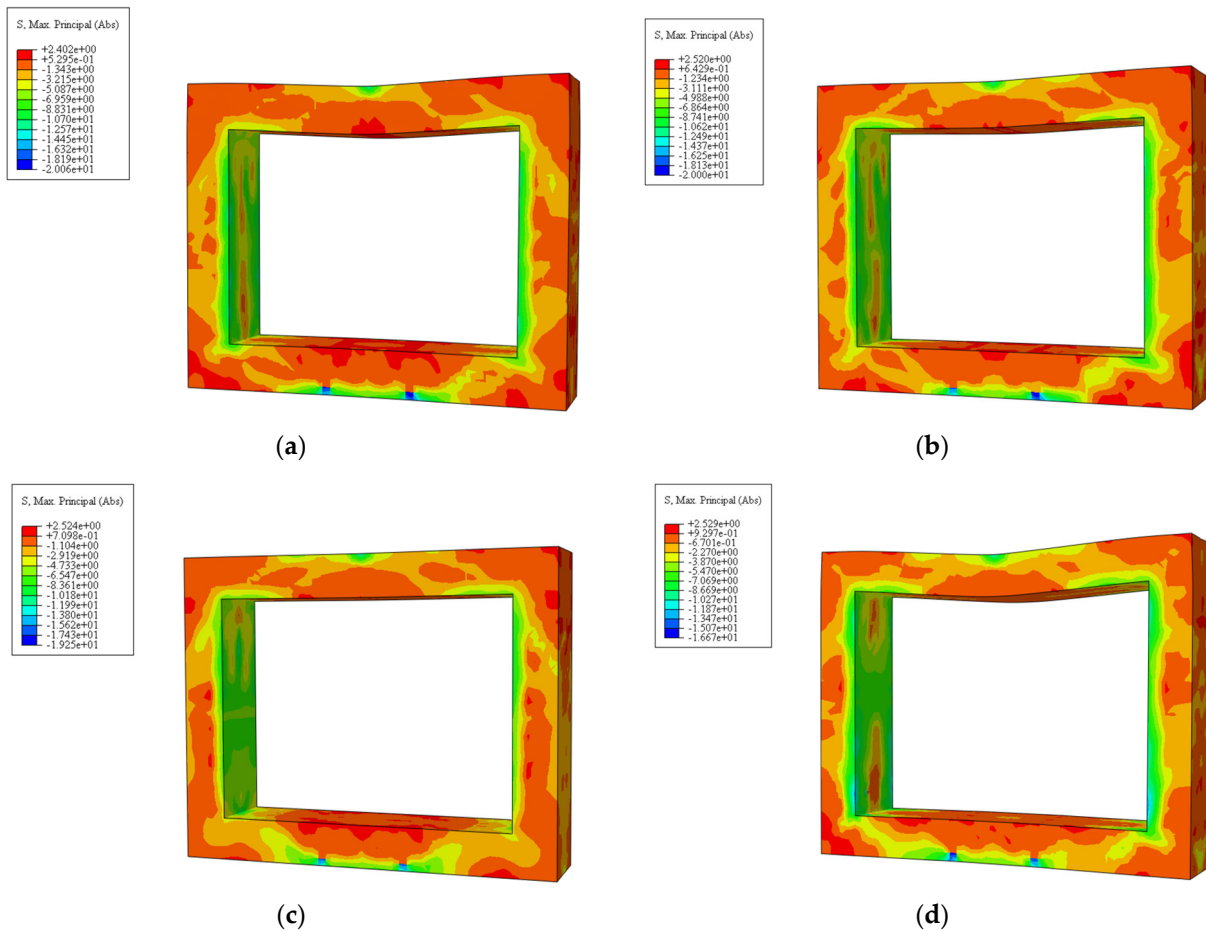


Figure 7. Distribution of maximum principal stress of pipe with different corrosion depths: (a) A1 pipe; (b) B1 pipe; (c) B2 pipe; (d) B3 pipe.

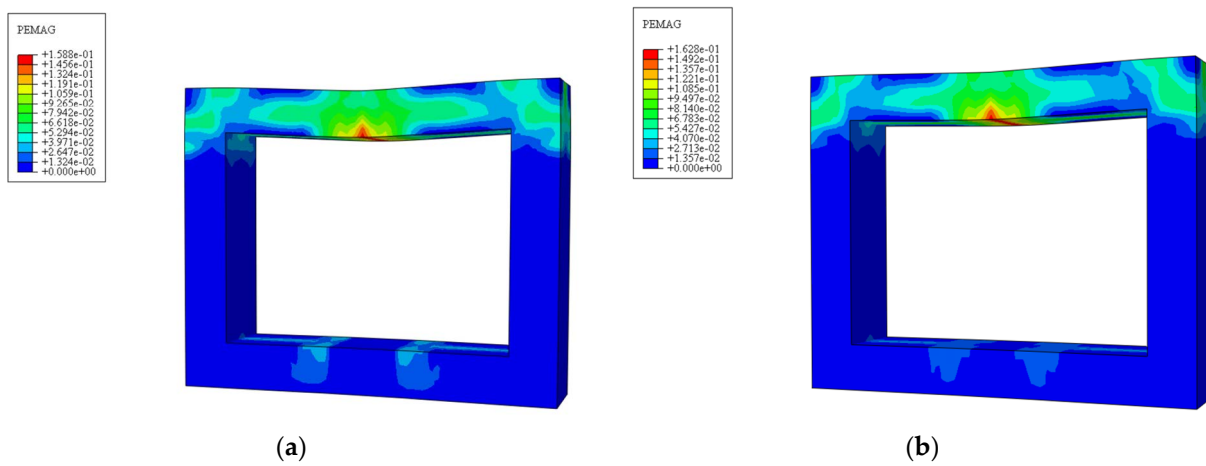


Figure 8. Cont.

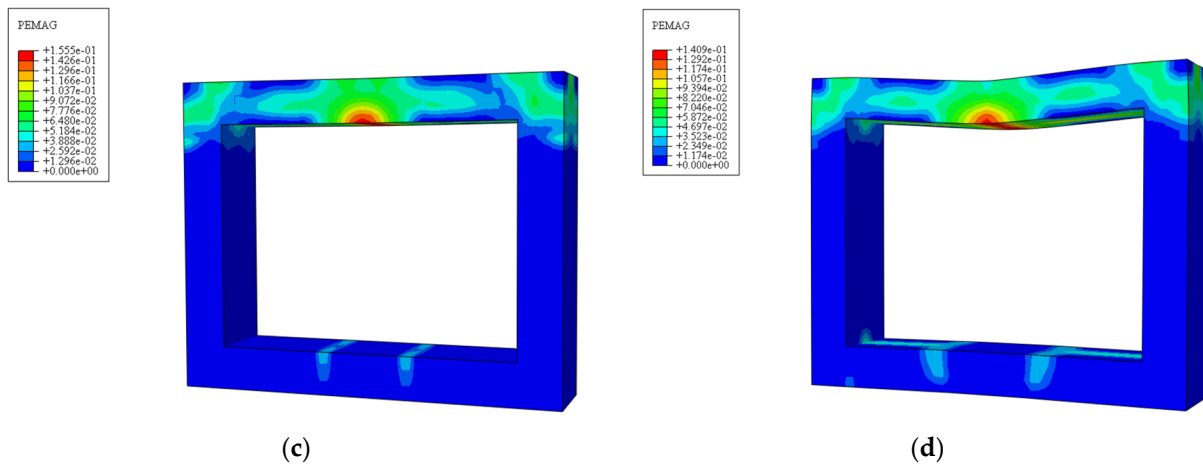


Figure 8. Plastic strain nephogram of pipe with different corrosion depths: (a) A1 pipe; (b) B1 pipe; (c) B2 pipe; (d) B3 pipe.

As shown in Figure 8a–d, the position and area of the plastic strain area of the pipe with different corrosion depths is almost unchanged, and the maximum plastic strain area is in the middle of the top span of the pipe. With the increase of corrosion depth, the development of the plastic strain area is from the top of the pipe to the side of the pipe, from the middle of the span to both sides. It can be concluded that, when the corrosion depth of the pipe is less than the thickness of the protective layer, the change of the corrosion depth has little effect on the plastic deformation area of the pipe, and the maximum plastic deformation is in the middle of the pipe top span. Based on the above rules, the numerical simulation results are in good agreement with the experimental results.

According to the simulation results, the reaction force and the vertical displacement of the simulated pipe loading reference point are derived, and the load-displacement curve is obtained, as shown in Figure 9. The curve trend of pipe simulation with different corrosion depths is the same: the load-displacement curve of the pipe is a straight line in the early stage of loading, and the load and displacement of the pipe are in direct proportion. This section corresponds to the uncracked stage and crack development stage of the pipe. In the early part of this stage, the pipe did not crack and showed elastic deformation. With the increase of displacement, the concrete in the tensile zone developed fine cracks, the pipe structure was not damaged, and the pipe was in good working condition. Then the bearing capacity of the pipe section continues to increase with the increase of the displacement, and stops growing when the ultimate bearing capacity of the pipe section is reached. The slope of the load-displacement curve decreases with the increase of the displacement, and the growth rate of the bearing capacity of the pipe slows down. Corresponding to the pipe failure stage in the test, the pipe crack gradually develops from the tensile zone to the compressive zone at this stage. The load on the pipe is mainly borne by the steel bar, the deformation of the steel bar increases, the pipe structure is destroyed, and the bearing capacity of the pipe is reduced. When the load reaches the ultimate bearing capacity of the pipe, with the increase of displacement, the load of the pipe is almost unchanged or decreases slowly. At this time, the pipe structure has been completely destabilized and the pipe has lost its bearing capacity.

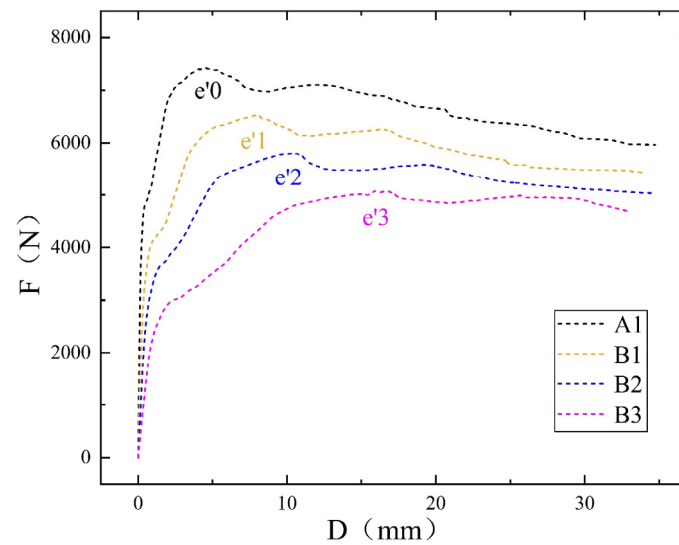


Figure 9. Numerical simulation load-displacement curves of pipes with different corrosion depths.

3.2.2. Analysis of Numerical Simulation Results of Pipe Load-Displacement Curve

The numerical simulation results of the ultimate bearing capacity of the pipe and the corresponding displacement are shown in Table 6. From the data analysis in the table, it can be seen that, with the increase of the corrosion depth, the ultimate bearing capacity of the pipe decreases, and the corresponding displacement of the ultimate bearing capacity of the pipe increases, indicating that, the thinner the inner wall of the pipe, the weaker the bearing performance, and the damage has occurred before the pipe reaches the ultimate bearing capacity.

Table 6. Numerical simulation of ultimate bearing capacity of pipes with different corrosion depths.

| Serial Number | The Ultimate Bearing Capacity Corresponds to the Displacement (mm) | Ultimate Bearing Capacity (N) |
|---------------|--|-------------------------------|
| A1 | 4.51 | 7421.94 |
| B1 | 7.97 | 6523.86 |
| B2 | 10.50 | 5898.35 |
| B3 | 15.93 | 5073.23 |

3.2.3. Comparative Analysis of Experimental and Numerical Simulation Results

As shown in Figure 10, it can be determined that the ultimate bearing capacity–corrosion depth curve obtained by the numerical simulation of the pipe section is straight, that is, the ultimate bearing capacity of the pipe decreases uniformly with the increase of the corrosion depth of the pipe. The numerical simulation results of the ultimate bearing capacity of pipes with different corrosion depths are compared with the experimental values. The simulation value of the ultimate bearing capacity of non-destructive pipes is 7421.94 N, which is smaller than the experimental value, and the error between the simulation value and the experimental value is only 4.47%. When the corrosion depth of the pipe is 2.5 mm, the simulated ultimate bearing capacity of the pipe is 6423.86 N, which is 12.10% lower than that of the non-destructive pipe joint, and the error with the experimental value is 1.31%. When the corrosion depth of the pipe is 5 mm, the simulated ultimate bearing capacity of the pipe is 5898.35 N, which is 20.52% lower than that of the non-destructive pipe, and the error with the experimental value is 5.05%. When the corrosion depth of the pipe is 7.5 mm, the corrosion depth is equal to the thickness of the inner protective layer of the pipe. The simulated ultimate bearing capacity of the pipe is 5073.23 N, which is 31.64% lower than that of the non-destructive pipe, and the error with the experimental value is 5.67%. In summary, the error between the simulated value

and the experimental value of the ultimate bearing capacity of the pipe under TEB test conditions is small (within 6%) and the accuracy of the simulated value is high.

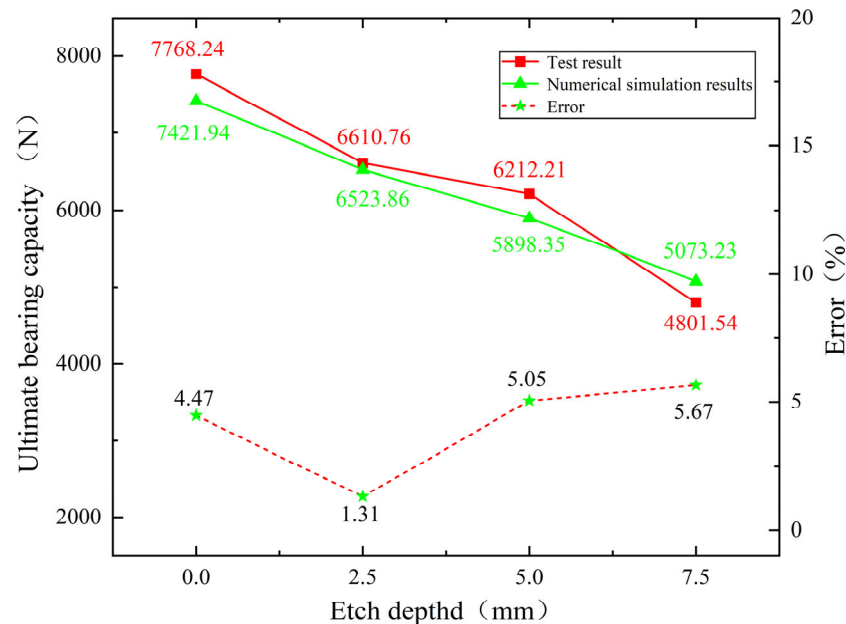


Figure 10. Comparison between simulated and experimental values of ultimate bearing capacity of corroded pipe.

4. Conclusions and Prospects

The main conclusions of this paper are:

1. The ultimate bearing capacity of pipe is usually measured by a TEB test. The failure mode of rectangular reinforced concrete pipe can be divided into three stages: uncracked stage, crack development stage and failure stage. The load on the pipe in the uncracked stage increases proportionally with the displacement. The load on the pipe in the crack development stage increases with the increase of the displacement. The curvature of the load-displacement curve decreases, and the cracks appear on the pipe wall and gradually develop.
2. The decrease of ultimate bearing capacity of corroded reinforced concrete pipes is manifested by thinning of the pipe wall thickness. Only considering the corrosion thinning effect of the pipe wall, when the corrosion depth is less than or equal to the thickness of the concrete protective layer inside the pipe wall, the ultimate bearing capacity of the pipe decreases with the increase of the corrosion depth. When the corrosion depth is equal to the thickness of the protective layer, the experimental value and numerical simulation value of the ultimate bearing capacity of the pipe decrease by 31%, and the error between the two is less than 10%, which proves that the corrosion depth has a great influence on the mechanical properties of the pipe.

In this paper, the mechanical properties of rectangular reinforced concrete structures with corrosion defects were studied. The reduction of material strength in corrosion conditions was not considered. Further research needs to be carried out in combination with material properties. In addition, the actual stress of the pipe is more complex, and the soil load and live load need to be considered in the tests.

Author Contributions: Conceptualization, Z.M.; Data curation, Z.M.; Formal analysis, Z.M.; Funding acquisition, P.Z.; Investigation, Z.M.; Methodology, Z.M.; Validation, Z.M.; Visualization, P.Z.; Writing—original draft, Z.M., P.Z. and C.Z.; Writing—review and editing, Z.M. All authors have read and agreed to the published version of the manuscript.

Funding: This paper is supported by Science and Technology Project of State Grid Corporation of China (No. 5200-202029144A-0-0-00).

Institutional Review Board Statement: Not applicable.

Informed Consent Statement: Not applicable.

Data Availability Statement: Some or all data that support the findings of this study are available from the corresponding author upon reasonable request.

Conflicts of Interest: The authors declare no conflict of interest.

References

1. Ma, B.S.; Najafi, M. Development and applications of trenchless technology in China. *Tunn. Undergr. Space Technol.* **2008**, *23*, 476–480. [[CrossRef](#)]
2. Tian, Q.; Xue, G.Z.; Tian, J.B.; Zheng, L.N. Economic benefits research of urban utility tunnel. *Chin. J. Undergr. Space Eng.* **2015**, *11*, 373–377.
3. Guan, X. Cost comparison of tunnel utility-tunnel with traditional tube-based tunnel—Taking the tunnel utility-tunnel of west zone of Zhongguancun for the example. *Constr. Econ.* **2009**, *S1*, 339–342.
4. Liu, F. Finite-Element Simulation of the Releasing Process of Existing Stress in Concrete Structures by Drilling Hole Method. Master's Thesis, Northeastern University, Shenyang, China, 2009.
5. Wu, F.; Zhuo, Y.; Qiu, S. Measurement of existing stress in prestressed concrete piles. *Port Waterw. Eng.* **2012**, *469*, 31–34.
6. Li, X.P.; Zeng, Y.X.; Luo, J.B. On finite element analysis of existing stresses of prestressed box girder measured by hole drilling method. *Shaanxi Archit.* **2013**, *39*, 147–148.
7. Fan, H.; Liu, B.; Fan, Z.; Wang, C. Model test with similar material and numerical simulation of culvert with high fills. *J. Jilin Univ. (Eng. Technol. Ed.)* **2008**, *136*, 399–403.
8. Wang, W.L.; Zhao, D.J.; Wang, L. Influence of lateral fill load on foundation bearing capacity of culvert. *China J. Highw. Transp.* **2010**, *23*, 1–6.
9. Cao, S.Y.; Zhu, B.L. Performance of corroded concrete and reinforced concrete. *J. Tongji Univ. (Nat. Sci.)* **1990**, *2*, 239–242.
10. Moradi, M.; Valipour, H.; Foster, S. Reserve of Strength in Inverted U-Shaped RC Culverts: Effect of Backfill on Ultimate Load Capacity and Fatigue Life. *J. Bridge Eng.* **2016**, *21*, 04015051.1–04015051.10. [[CrossRef](#)]
11. Abolmaali, A.; Garg, A.K. Effect of Wheel Live Load on Shear Behavior of Precast Reinforced Concrete Box Culverts. *J. Bridge Eng.* **2008**, *13*, 93–99. [[CrossRef](#)]
12. Zhu, Z.; Zhang, P.; Ma, B.; Zeng, C.; Zhao, Y.; Wang, F.; Li, Z.; Xiang, W.; Ariaratnam, S.T.; Yan, X. Quantitative model for residual bearing capacity of corroded reinforced concrete pipe based on failure mode. *Tunn. Undergr. Space Technol.* **2022**, *129*, 104675. [[CrossRef](#)]
13. Yang, K.D.; Fang, H.Y.; Li, B. Numerical study on concrete pipe corroded at crown under traffic load. *Chin. J. Undergr. Space Eng.* **2019**, *15*, 129–135.
14. Ma, Z.; Wu, H.G.; Shi, C.Z. Research on the cracking mechanism and simulation technology of steel-lined reinforced concrete penstock. *J. Tianjin Univ. (Sci. Technol.)* **2022**, *55*, 46–56.

Disclaimer/Publisher's Note: The statements, opinions and data contained in all publications are solely those of the individual author(s) and contributor(s) and not of MDPI and/or the editor(s). MDPI and/or the editor(s) disclaim responsibility for any injury to people or property resulting from any ideas, methods, instructions or products referred to in the content.